

Buoyancy driven flow in reactor safety

R. Vaibar^{a,b,*}, T. Höhne^b

^a*Institute of Fluid Mechanics, TU Dresden, George-Bähr-Strasse 3c, D-01062 Dresden, Germany*

^b*Institute of Safety Research, Forschungszentrum Dresden-Rossendorf, Bautzner Landstrasse 128, 0138 Dresden, Germany*

Received 5 September 2008; received in revised form 18 December 2008

Abstract

Buoyancy driven flow is often found in many engineering applications such as the mixing process of fluids, which have different densities. The aim of this study is to simulate mixing of borated and unborated water, an issue which is relevant to the analysis of the safety of nuclear reactors. The degree of mixing of weakly and highly borated coolant is a critical issue with respect to reactivity of the reactor core. Therefore, a combined numerical and experimental study of buoyant mixing processes has been performed. The numerical studies on different types of grid show, that the main influence to the description of the mixing processes is the simplification of the flow domain. In the case when the proper flow domain is used, a better agreement between the numerical and experimental results can be achieved.

© 2009 University of West Bohemia. All rights reserved.

Keywords: buoyancy, turbulence modelling, ROCOM, passive scalar diffusion

1. ROCOM test facility

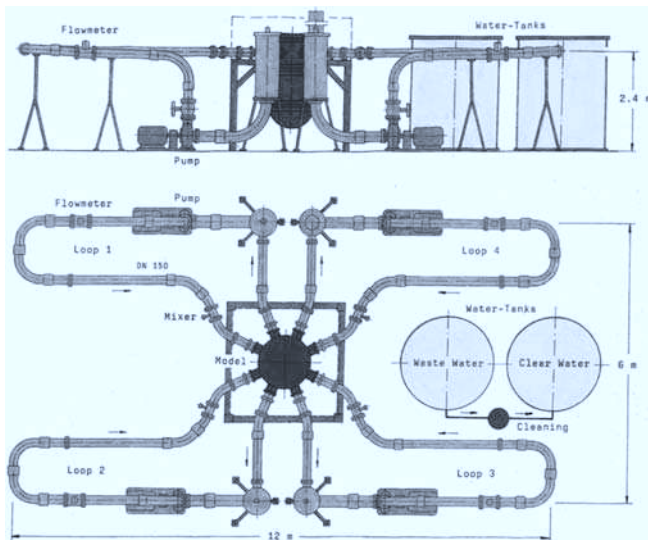
The test facility ROCOM (Rossendorf Coolant Mixing Model) was constructed to investigate coolant mixing in the downcomer of the pressure vessel of pressurized water reactors (PWR). ROCOM is a 1 : 5 scale model of the PWR KONVOI nuclear reactor. The test facility was designed for the investigation of a wide spectrum of mixing scenarios [1, 2, 3]. The experiments have been performed to measure the time-dependent distribution of transport variables such as coolant temperature and boron concentration inside the reactor pressure vessel. The leading input variables are the time history of the flow rates in the four loops of the primary circuit as well as the coolant temperature or boron concentration at the inlet nozzles, respectively. The differences in either boron concentration or coolant temperature are modeled by means of a salt tracer solution, which influences the electrical conductivity. The test facility is equipped with wire-mesh sensors that allow a high resolution measurement of the transient tracer concentration in space and time.

1.1. Design Parameters

The design parameters of the test facility are presented in the following table together with the data of the original reactor (Comparison original PWR-ROCOM with water at 20C)

*Corresponding author. Tel.: +420 608 579 559, e-mail: roman.vaibar@tu-dresden.de.

value	unity	original	ROCOM
inner diameter of the pressure vessel	mm	5 000	1 000
height of the pressure vessel	mm	12 000	2 400
inner diameter of the inlet nozzle	mm	750	150
width of the downcomer	mm	315	63
coolant flow rate per loop	m ³ /h	23 000	350 max., 185 nominal
coolant inlet velocity	$\frac{m}{s}$	14.5	5.5 max., 2.91 nominal
velocity in the downcomer	$\frac{m}{s}$	5.5	2.1 max., 1.1 nominal
Reynolds-number in the inlet nozzle	–	$8.4 \cdot 10^7$	$8.3 \cdot 10^5$ max., $4.4 \cdot 10^5$ nominal
Re downcomer	–	$2.7 \cdot 10^7$	$2.6 \cdot 10^5$ max., $1.4 \cdot 10^5$ nominal
Re original/Re ROCOM	–	1	100 max., 190 nominal
coolant travelling time original/ROCOM	–	1	1 (nominal)



a) Schema of the ROCOM test facility



b) Plexiglas model of reactor pressure vessel

Fig. 1. ROCOM test facility

1.2. Buoyancy related mixing experiments

The mixing of slugs of water with different physical properties is very important for situations where pre-stressed thermal shock could affect the structural integrity of the reactor. When the emergency core cooling system is activated during a loss-of-coolant accident, cold water is injected into hot water, which is present in the cold leg and downcomer. Due to the large temperature differences, thermal shocks are induced at the reactor pressure vessel wall. Temperature distributions near the wall and temperature gradients in time are known to be important in the assessment of thermal stresses. This temperature distribution is highly influenced by the mixing of the injected emergency core cooling water with the ambient higher temperature water, which is making its way through the primary circuit. Investigations of the process of turbulent mixing,

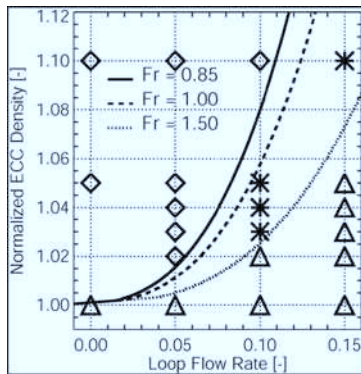
which occurs under the influence of buoyancy forces that arise from the temperature differences can contribute to the assessment of the thermal loading of the vessel wall.

1.3. Boundary conditions for the ROCOM experiments

The goal of the experiments was the generic investigation of the influence of the density difference between the primary loop inventory and the emergency core cooling water on the mixing in the downcomer. A key aim was to find the conditions at which the transition between momentum controlled and buoyancy driven mixing occurred. To separate the density effects from the influence of other parameters, a constant flow in the loop with the emergency core cooling injection nozzle was assumed in this study. The flow rate was varied in the different experiments between 0 and 15 % of the nominal flow rate, i.e. it was kept within the limits of the natural circulation regime. The pumps in the other loops were switched off. The density difference between emergency core cooling and loop water was varied between 0 and 10 %. The normalized density is defined as the ratio between emergency core cooling water density and density of fluid in the circuit. In all experiments, the volumetric flow rate of the emergency core cooling injection system was kept constant and all other boundary conditions are identical. Altogether 21 experiments have been carried out.

Due to the fact, that the test facility cannot be heated up, it was necessary to simulate the density differences that were caused by the fluid temperature and this was achieved by adding sugar to the water, which is injected into the cold leg. Observations of the mixing of the emergency core cooling water was made by adding a tracer through small amounts of sodium chloride.

1.4. Froude number in ROCOM vessel



The Froude number was used for characterisation of flow in the ROCOM vessel, which had the form:

$$Fr = \frac{v_{in}}{\sqrt{gs \frac{\rho_{in} - \rho_a}{\rho_{in}}}}, \quad (1)$$

v_{in} is the velocity at the reactor inlet (combined loop and ECC flow), g is the gravitational acceleration, s is the length of the downcomer, ρ_{in} the density of the incoming flow, calculated with the assumption of homogeneous mixing between ECC and loop flow, and ρ_a the density of the ambient water in the downcomer.

All density dominated experiments are located to the left of the isoline $Fr = 0.85$ and all momentum dominated experiments are located to the right of the iso-line $Fr = 1.50$. These two numbers are critical Froude numbers separating the two flow regimes for the ROCOM test facility. The transition region is located between these two values.

1.4.1. Experiment without density difference

Experiments were performed on the ROCOM test facility without any density difference effects to serve as control or reference experiments, which could be used to gauge the influence of the buoyancy forces. Fig. 2 visualises the the tracer concentration in ROCOM test facility for the control case no density difference 2a on the left hand side and a 10 % density difference 2b case on the right, the pump was operating at 15 % of the nominal flow rate.

At the upper downcomer sensor, the emergency core cooling water (injected in each experiment

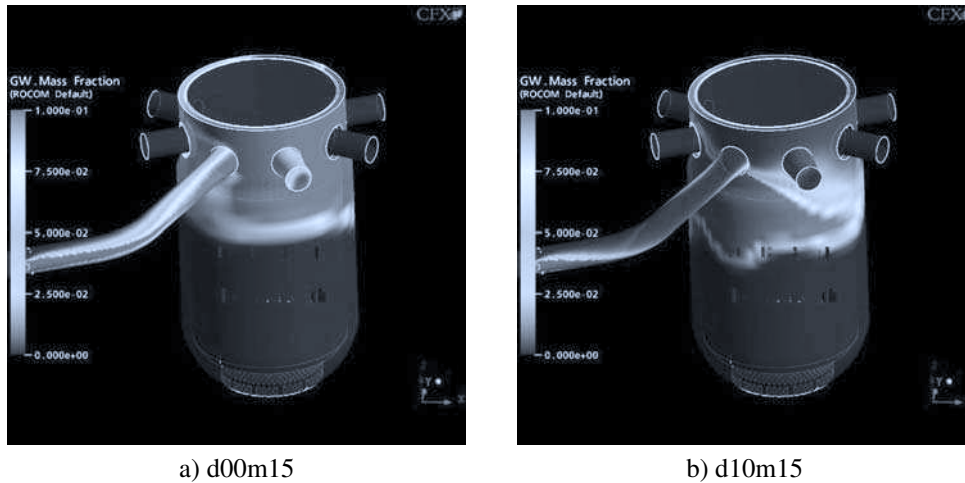


Fig. 2. ROCOM simulations at $T = 15$ [s], with nominal flow rate $m_{ratio} = 15\%$

from $t = 5$ to $t = 15$ s) appears directly below the inlet nozzle. Due to the momentum created by the pump, the flow entering the downcomer is divided into two streams flowing right and left in a downward directed helix around the core barrel. At the opposite side of the downcomer, the two streaks of the flow fuse together and move down through the measuring plane of the lower downcomer sensor into the lower plenum. Almost the whole quantity of emergency core cooling water passes the measuring plane of the lower downcomer sensor at the side opposite to the azimuthal position of the affected loop. The velocity field responsible for the observed tracer distribution is typical for single-loop operation. It has its maximum at the opposite side of the downcomer and a minimum at the azimuthal position of the running loop, which has been found in velocity measurements by means of a laser-Doppler anemometer (LINK) at the ROCOM test facility.

1.4.2. Experiment with a density difference of 5 %

Fig. 3 shows an experiment where there was a density difference of 5 % between the slug of emergency core cooling water in the cold leg and the fluid in the reactor. The flow rate in the cold leg was again set at 5 % of the nominal flow rate.

One part of the emergency core cooling water follows the stream lines of the momentum driven flow field (derived from the pump) and the other part directly falls down due to the internal momentum created by density differences. This case could be considered as an intermediate state between momentum and density driven flow. The experiment shown in Fig. 3 was therefore assigned to the transition region between the two flow regimes.

1.4.3. Experiment with a density difference of 10 %

On the right hand side of Fig. 2, the density difference between the injected emergency core cooling water and the primary loop coolant was specified as 15 % with the same nominal flow rate as for the control case. In this case, a streak of the water with the higher density is observed to travel through the downcomer below the inlet nozzle.

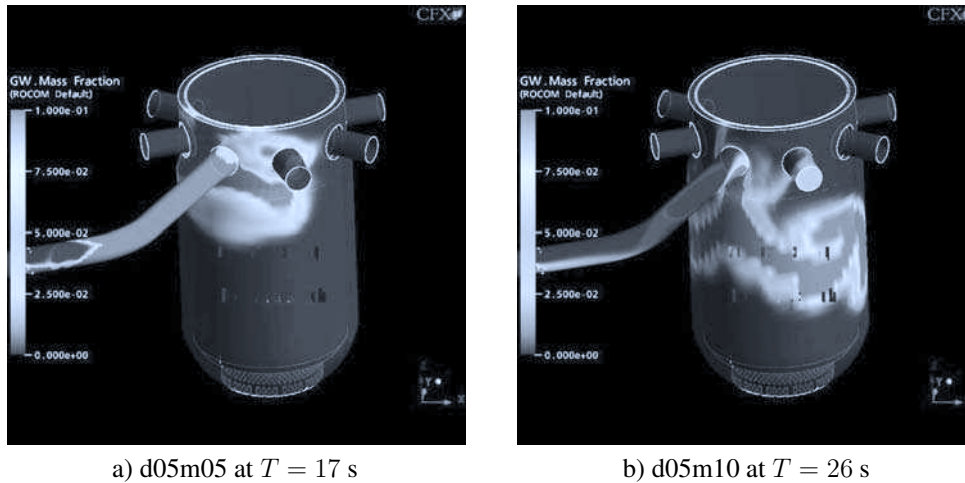


Fig. 3. ROCOM simulations with density difference $\Delta\rho = 5\%$ and nominal mass flow rate $m_{ratio} = 5\%$

At the upper sensor, the emergency core cooling water covers a much smaller azimuthal sector in the downcomer. The density difference partly suppresses the propagation of the emergency core cooling water in azimuthal direction. The emergency core cooling water falls down in an almost straight streamline and reaches the lower downcomer sensor directly below the affected inlet nozzle. Only later, does coolant, which contains any emergency core cooling water, appear at the opposite side of the downcomer. The maximum concentration values observed at the two downcomer sensors are in the same range as in the case without density differences, i.e. 20.1 % and 9.7 % from the initial concentration in the emergency core cooling water tank.

The visualizations of the behaviour of the emergency core cooling water in the downcomer reveals that in case of momentum driven flow, the emergency core cooling water covers nearly the whole perimeter of the upper sensor and passes the measuring plane of the lower sensor mainly at the opposite side of the downcomer. When the density effects are dominating, the sector at the upper measuring device covered by the emergency core cooling water is very small. The emergency core cooling water falls straight down and passes the sensor in the lower part of the downcomer below the inlet nozzle of the working loop.

2. Numerical simulations at the ROCOM test facility — case d10m15

2.1. Description of calculation

The case d10m15, which means density difference $d10 \approx \Delta\rho = 0.10$ and $d10 \approx \Delta\rho = 0.10$, was chose for the study the flow behaviour in the transition region between the momentum and buoyancy dominated flow type. For simulation was used the different type of grid , which are shown in the Figure 4. The several type of turbulence models was used in the simulations [5].

- the standard $k - \epsilon$ turbulence model — member of two-equation family turbulence model, turbulent stress is modelled via the analogy with the laminar stress, where the turbulence viscosity is defined by the two scale parameters
- the standard Shear Stress Transport turbulence model — member of two-equation family turbulence model



a) part cold leg full ROCOM vessel b) full cold leg part ROCOM vessel c) full cold leg full ROCOM vessel

Mesh Statistics		Mesh Statistics		Mesh Statistics	
Number of Nodes:	2 015 568		153 576		2 117 619
Number of Elements:	4 121 284		554 444		4 120 541
Tetrahedral:	2 401 790		422 110		2 283 011
Wedges:	471 164		132 073		471 164
Pyramids:	26 854		261		27 210
Hexahedra:	1 221 476		0		1 339 156

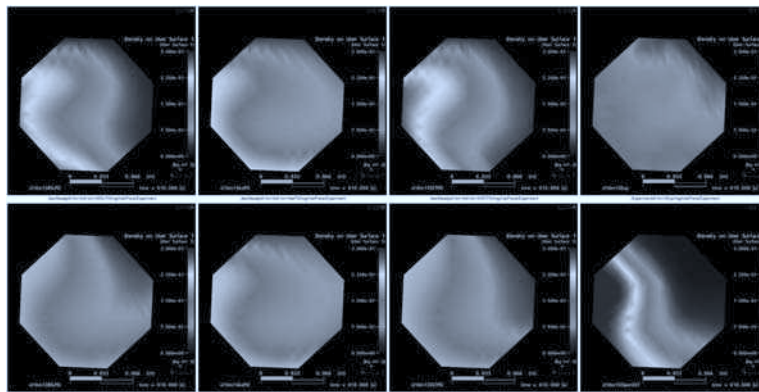
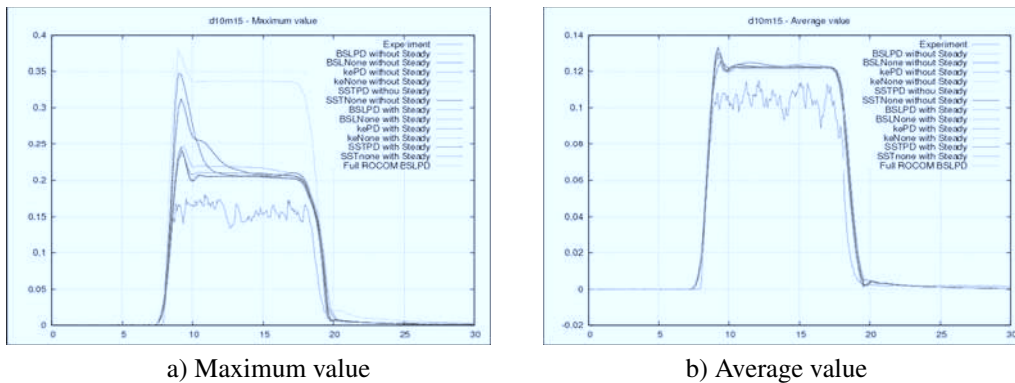
Fig. 4. The different meshes used to model the ROCOM test facility with mesh statistics

- the BSL Reynolds Stress model from the Reynolds stress turbulence model, where the turbulence stress is directly solved with the transport equations for all six components of the turbulence stress.
- the DES Detached Eddy Simulation model — combination of the two turbulence modelling approaches, the Large Eddy Simulation technique and the Reynolds Averaged Navier Stokes approach. In this case, the Shear Stress Transport model is used
- without turbulence model — laminar type of flow

- Initialization by the so-called *with Steady* state calculation was used. The Steady state initialization means that before starting the transient calculation a partial flow solution was obtained after 1000 iterations in which the steady state mode was selected. The Steady state calculation enabled the development of the main flow field in the simulation domain. Therefore, the velocity and pressure fields are resolved to there steady state forms and these fields are then used to initialise the transient calculation. The Shear Stress Transport turbulence model was chosen in Steady state precalculation.
- Initialization by the so-called *without Steady* state calculation meant that a zero state condition was used to initialise the velocity and pressure field. Thus, every disturbance of the main flow field must be resolved before the injection of the heavy water into Emergency Core Cooling pipe.
- The time step was set to $\Delta t = 0.1$ [s] and time duration was specified as $T_{\text{totaltime}} = 30$ s. The total time was applied due to the fact that the heavy water will leave the domain depicted in Fig. 4c within 30 s of the injection and the main focus of this study is the behaviour the slug in the inlet nozzle wire-mesh sensor region.

- The impulse of the injection of heavy water through the Emergency Core Cooling pipe was defined via the step function $stepfunction = 1$ in time $T \in \langle 5, 15 \rangle$.
- The inlet velocity in Emergency Core Cooling pipe was specified via the expression $speedECC = stepfunction * 0.64297 \text{ m} \cdot \text{s}^{-1}$, where the nominal flow velocity in ECC pipe is $v_{nomECC} = 0.64297 \text{ m} \cdot \text{s}^{-1}$.
- The inlet velocity in the cold leg was setup via the expression $inCL1 = 2.91 * mratio * 1 \text{ m} \cdot \text{s}^{-1}$, where the nominal flow velocity in the cold leg is $v_{nom} = 2.91 \text{ m} \cdot \text{s}^{-1}$.
- The *No – Slip* boundary condition was used on the wall boundary conditions.

2.2. Results at the inlet nozzle position



c) Inlet sensor position comparison – case d10m15

Fig. 5. Case d10m15 characteristic of comparison on inlet nozzle position

The traces of the maximum value of the slug concentration are found in Figure 5a, where the value was measured by the inlet nozzle wire mesh sensor and determined by $Max = \max_i C_i$, $i = 1, \dots, 216$. From comparisons made between the simulations and the experiment, it is clearly seen that there is an over-prediction of the maximum value of the concentration for the earlier case where only a partial cold leg was used. The remaining traces of the simulations presented in relation to the study with full cold leg and only part of the ROCOM vessel match

the evolution of maximum concentration value in the experiments for all applications of the turbulent models considered. The discrepancies of the overprediction in maximum value in the case without the steady state initialization such as the SST and BSL turbulence models still result in the poor development of the flow field in the flow region reconsidered. The time delay used in the calculation before the starting injection is 5 [s] and this 5 [s] is not sufficient to create proper flow field in the cold leg. When the steady state initialization is used, it is clearly seen that this overprediction disappears.

Figure 5b presents the traces for the averaged-value of the concentration at the inlet nozzle wire mesh sensor, $Ave = \frac{1}{216} \sum_{i=1}^{216} C_i$. The averaged-value curves show that the simulation and the experimental data have the similar values of C_{AveEXP} cca 0.107 C_{AveSim} cca 0.12. This is expected as the continuity equation conserves the transport of mass and averaged-value shows that the movement of the slug of water is in agreement with the movement of slug in the experiment and simulation.

The contour plots in Figure 5c enable the comparison of the concentration distribution at the cold leg inlet plane at time $T = 10$ s. By time $T = 10$ [s], the slug of the injected water reaches the position of the cold leg inlet wiremesh sensor. The scale, which is used in the comparison view is $C \in \langle 0, 0.3 \rangle$.

The resultant figures are show in a matrix of the form:

FP BSL	FP $k - \epsilon$	FP SST	PF BSL	PF DES	Experiment
FPS BSL	FPS $k - \epsilon$	FPS SST	PFS $k - \epsilon$	PF laminar	PF SST

where the description of the result is based on the key

- first letter is based on the type of the cold leg geometry P – Partial, F – Full cold leg,
- second letter is based on the type of the ROCOM vessel geometry P – Partial, F – Full,
- third letter is S in the case when the initialization with the Steady state was used in simulation,
- the name of the turbulent model used in simulation.

It is immediately apparent that the slug stratification in the simulation for the partial cold leg and full ROCOM vessel is very poor. Comparing the partial cold leg simulation (PF XXX results on the Figure 5c) with the contours of the measured data, the slug has huge overprediction on the left side and on the middle and right side of the inlet an underprediction of the concentration is depicted. This behaviour is found in all of the turbulence models used, which indicates that the stratification effects are not captured by the modelling by purely using the turbulent flow model. Nevertheless, these stratification effects are caused by some physical phenomena in the ROCOM test facility, where the domain simplification by considering only a partial cold leg maybe the underlying cause of the poor slug stratification. The physical simplification in the type of simulation with partial cold leg utilises the principle of the uniform inlet velocity and this is not valid in cases where higher flowrates are used in the cold leg. Conversely, all the cases where the full cold leg is modelled (FPX XXX result on the Figure 5c), the stratification of the slug is much better with high concentrations on the left side of the inlet and lower concentrations on the right. The effect of the partial solution of the steady state flow field on the transient solution is seen when we compare the contours depicted in the first against those depicted in the second row. However, for all the different turbulence models used in the grid with full cold leg simulation the concentration stratification has a “C” structure formation. The lowest concentrations are found on the top right side of the cold leg. However, in the case which was solved with the SST model and without steady state initialization, the “C” structure has rotated clockwise so that the lower concentration region is located on the right side. Note that the

time of first detection of the higher concentration and the duration of the impulse of the slug is exactly same in the experiments as it is in each simulation.

2.3. Comparison results

Comparison study was performed that was based on the following parameters

$$Error1(t) = \sum_{i=1}^{216} (C_{CFX}(t) - C_{EXP}(t))^2, \quad (2)$$

$$Maximum(t) = \max_{i=1}^{216} C(t), \quad (4)$$

$$ErrorGlobal = \sum_{t=0}^{30} Error1(t) \quad (3)$$

$$MaximumGlobal = \max_{t=0}^{30} Maximum(t), \quad (5)$$

$$MaxOverprediction = \frac{MaximumGlobal(CFX)}{MaximumGlobal(EXP)} \quad (6)$$

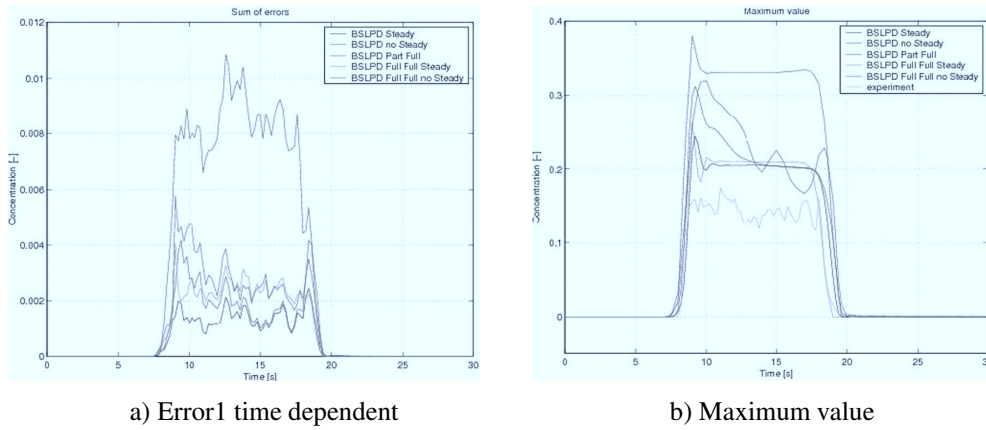


Fig. 6. Case d10m15 with Reynolds Stress turbulence Model with the Baseline definition

Figure 6 present the results for case d10m15 where the Reynolds Stress turbulence Model was used with the Baseline definition for several grids and initialization procedures. The acronyms in the legend are defined as:

- *BSLPD Steady* and *BSL no Steady* — simulation on grid with respect to the full cold leg geometry and partial ROCOM vessel, with and without Steady state initialization
- *BSLPD Part Full* — simulation on grid with respect to the partial cold leg geometry and full ROCOM vessel
- *BSLPD Full Full Steady* and *BSLPD Full Full no Steady* — simulation on grid with respect to the full cold leg geometry and full ROCOM vessel, with and without Steady state initialization.

Figure 6a presents the time dependency of the error defined by the formula (2). It is apparent that the solution *BSLPD Part Full* has the most significant errors. The solution, which was performed on the grid with respect the full cold leg geometry still produces the large errors, but the range of the errors is decreased by factor of ≈ 3 . Figure 6b depicts the time dependency of the maximum value that occurs in the simulation and experiment. From the maximum value, it is observable that the simulation *BSLPD Part Full* has the largest value. When the simulations are initialized with the partial Steady state solution, *BSLPD Steady* and *BSLPD Full Full Steady*, the over-prediction of the concentration is not as the *BSLPD Part Full*, particularly after the initial contact of the slug at the inlet sensor position.

Table 1. Global characteristic case d10m15 RSM BSL turbulence model

Simulation	ErrorGlobal [-]	MaximumGlobal [-]	MaxOverprediction [%]	Order
<i>BSLPD Steady</i>	0.075 7	0.244 2	1.396 2	1
<i>BSLPD no Steady</i>	0.110 4	0.312 3	1.785 7	2
<i>BSLPD Part Full</i>	0.415 8	0.380 1	2.173 2	5
<i>BSLPD Full Full Steady</i>	0.125 3	0.263 3	1.505 2	3
<i>BSLPD Full Full no Steady</i>	0.157 8	0.319 6	1.827 6	4
<i>experiment</i>	0	0.174 9	1	–
<i>experiment +3%</i>	0	0.204 9	1.171 5	–

Table 2. Global characteristic case d10m15

Simulation	ErrorGlobal [-]	MaximumGlobal [-]	MaxOverprediction [%]	Order
<i>BSLPD Steady</i>	0.075 7	0.244 2	1.396 2	3
<i>SSTPD Steady</i>	0.089 1	0.239 7	1.370 3	4
<i>kePD Steady</i>	0.059 5	0.235 1	1.344 1	1
<i>BSLPD no Steady</i>	0.110 4	0.312 3	1.785 7	5
<i>SSTPD no Steady</i>	0.122 4	0.349 4	1.997 7	6
<i>kePD no Steady</i>	0.073 4	0.246 3	1.408 5	2
<i>BSLPD Part Full</i>	0.415 8	0.380 1	2.173 2	13
<i>BSLPD Full Full Steady</i>	0.125 3	0.263 3	1.505 2	7
<i>DESPD Full Full Steady</i>	0.142 3	0.293 7	1.679 5	8
<i>SSTPD Full Full Steady</i>	0.144 4	0.291 4	1.666 3	9
<i>Lam Full Full Steady</i>	0.525 3	0.532 8	3.046 1	14
<i>BSLPD Full Full no Steady</i>	0.157 8	0.319 6	1.827 6	12
<i>DESPD Full Full no Steady</i>	0.151 1	0.263 2	1.505 1	10
<i>SSTPD Full Full no Steady</i>	0.153 2	0.259 9	1.485 8	11
<i>experiment</i>	0	0.174 9	1	–
<i>experiment +3%</i>	0	0.204 9	1.171 5	–

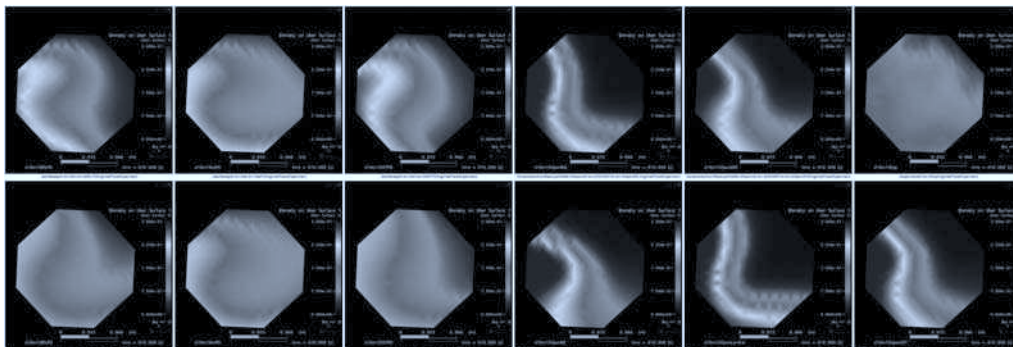
In Table 1 the global characteristics of each simulation are presented. Note that only the Reynolds Stress turbulence Model with the Baseline definition was used in obtaining these values. As from the graphical result of Maximum value and the Error1 time dependency given in Figure 6, the global characteristics also indicate that the configuration modelled and the initialisation procedure have a significant effect on the transport of the tracer.

The closest simulation to the experiment is the simulation with the minimal value of the *Error-Global*, which is the method *BSLPD Steady*. Both simulations with the full cold leg and full ROCOM vessel *BSLPD Full Full XXX* show good agreement with experimental data.

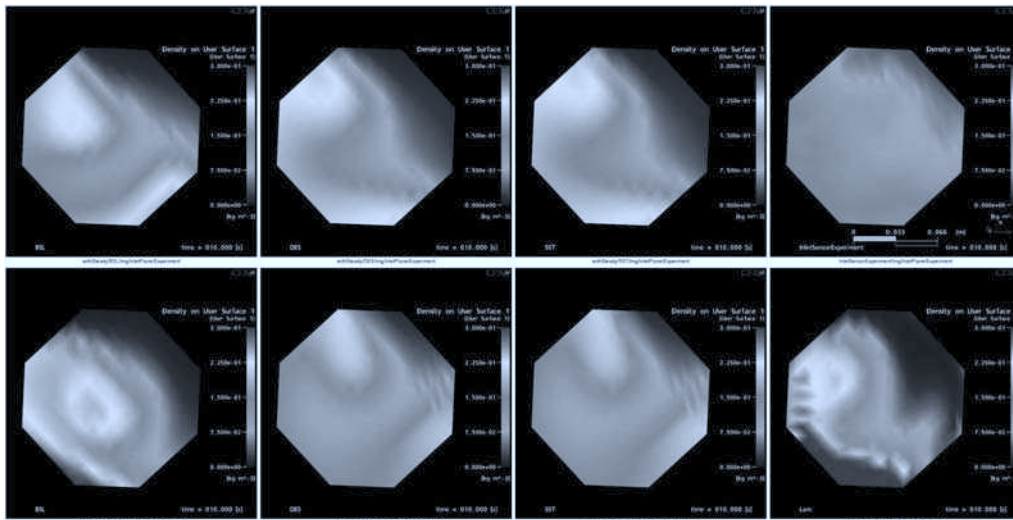
The prediction of the maximum concentration is stored in the column called *MaximumGlobal*. This property also found the *BSLPD Steady* as the best option from the selected model configurations.

The definition of the over-prediction is stored in the column *MaxOverprediction*. This property also indicated that the most appropriate technique from the compared cases was the *BSLPD Steady*.

In Table 2 the global characteristics of each simulation are presented, with different turbulence model. The results which take into account the simulation of the flow in the full cold leg had much better agreement the simulation with part cold leg. The decencies on the difference turbulence model could be found but with comparison to the influence of the full cold leg simulation this discrepancies are negligible. On the same type of simulation (same type of grid and same type of initialization) give the different turbulence method the very similar results and the discrepancies is to the experimental data are in the same order.



a) Part cold leg full ROCOM vessel and full cold leg part ROCOM vessel



b) Full cold leg full ROCOM vessel

Fig. 7. Comparison results at the Inlet nozzle position

The resultant figure are shown in a matrix of the form:

Figure 7a:

FP BSL	FP $k - \epsilon$	FP SST	PF BSL	PF DES	Experiment
FPS BSL	FPS $k - \epsilon$	FPS SST	PFS $k - \epsilon$	PF laminar	PF SST

Figure 7b:

FF BSLPD	FF kePD	FF SSTPD	experiment
FFS BSLPD	FFS kePD	FFS SSTPD	PF BSL

where the description of the result is based on the key

- first letter is based on the type of the cold leg geometry P – Partial, F – Full cold leg geometry,
- second letter is based on the type of the ROCOM vessel geometry P – Partial, F – Full,
- third letter is S in the case when the initialization with the Steady state
- the name of the turbulent model used in simulation.

From the comparison shown in the Figure 7a is very clear see that the good mixing and stratification in the full inlet cold leg found in the cases FP XXX occurs also in the cases FF XXX in Figure 7b. The effect of the partial solution of the steady state flow field on the transient solution is seen when we compare the contours depicted in the first against those depicted in the second row. However, for all the different turbulence models used in the grid with full cold leg simulation the concentration stratification has a “C” structure formation. The lowest concentrations are found on the top right side of the cold leg.

3. Conclusion

The ROCOM test facility was presented with flow characterization based on Froude number. Density related mixing flow condition was shown with the main characteristic of the flow type, momentum dominated and buoyancy dominated flow. The results were discuss on the case d10m15, which is in the transient region between the main flow type. The main reason from the simulations studies is that the neglecting the physical phenomena (short cold leg) has huge influence to the discrepancies between the simulations results and experimental data. The explanation of this phenomena is, that the flow with higher flow rate produce the different flow stratification in the input cold leg. The assumption of the unified inlet velocity on the position of inlet surface in case with the short cold leg is wrong. With the increasing of the flowrate in the cold leg this phenomane take higher influence as was found during comparison study. The discrepancies between the different turbulent models is not such significant and when is used the proper type grid the discrepancies are in the same order of magnitude. This behaviour was found through the whole experimental study, which cover the buoyancy dominated case, transient case and momentum dominated case.

Acknowledgements

This project is funded by the German Federal Ministry of Economics and Technology under contract number 150 1287.

References

- [1] S. Kliem, H.-M. Prasser, G. Grunwald, U. Rohde, T. Hhne, F.-P. Wei, ROCOM experiments on the influence of density differences on the coolant mixing inside the reactor pressure vessel of a PWR, Proc. Annula Meeting on Nuclear Technology 2002, 65–69, 2002.
- [2] H.-M. Prasser, G. Grunwald, T. Hhne, S. Kliem, U. Rohde, F.-P. Wei, Coolant mixing in a PWR — deboration transients, steam line breaks and emergency core cooling injection — experiments and analyses, Nuclear Technology, 37–56, 2003.
- [3] G. Grunwald, T. Hhne, S. Kliem, H.-M. Prasser, K.-H. Richter, U. Rohde, F.-P. Wei, Khlmitelvermischung in Druckwasserreaktoren — Teil 2, Experimentelle Ausrstung und Simulation der Vermischung, Report FZD-367, 2003
- [4] R. Vaibar, Numerical and experimental approach of turbulent buoyancy driven flow in reactor safety research, Ph.D. thesis, Pilsen, 2008.
- [5] ANSYS Europe Ltd., CFX 10.0 Documentation, Turbulence and near-wall modelling, 2005.